We are IntechOpen, the world's leading publisher of Open Access books Built by scientists, for scientists

4,800
Open access books available

122,000
International authors and editors

135M
Downloads

Our authors are among the

154
Countries delivered to

TOP 1%
most cited scientists

12.2%
Contributors from top 500 universities

CLARIVATE ANALYTICS BOOK CITATION INDEX INDEXED

WEB OF SCIENCE™

Selection of our books indexed in the Book Citation Index in Web of Science™ Core Collection (BKCI)

Interested in publishing with us?
Contact book.department@intechopen.com

Numbers displayed above are based on latest data collected.
For more information visit www.intechopen.com

6

Single-Phase Grid Connected Converters for Photovoltaic Plants

Emilio Lorenzani[1], Giovanni Franceschini[1], Alberto Bellini[2] and Carla Tassoni[1]
[1]*University of Parma, Italy*
[2]*University of Modena and Reggio Emilia, Italy*

1. Introduction

Among renewable energy sources photovoltaic systems are one of the most up to date solutions. However their diffusion is limited by relatively high cost in comparison with traditional energy sources. The downward tendency in the price of the PV (Photovoltaic) modules, together with their increasing efficiency, put solid-state inverters under the spot lights as the enabling technology for integrating PV systems into the grid.
This chapter will analyze the single-phase grid connected converter usually used in PV domestic rooftop applications.
There are two mandatory tasks in grid connected PV systems: the maximization of the energy extracted from the PV panels (1) and the use of a high efficiency topology for the power converter able to inject only active current into the grid (2), i.e. a pure sinusoidal current in phase with the grid voltage.
The first task will not be discussed in depth in this chapter and will be mentioned in section 2. The second task is accomplished by using a PLL (Phase Looked Loop) for the grid synchronisation (Chung, 2000), (Arruda et al., 2001), (Silva et al., 2004) and by designing a suitable current controller.
In three-phase converters current controllers in a rotating reference frame (d-q frame) are used that provide zero steady-state error and superior disturbance rejection. In single-phase converters achieving zero steady state error at grid frequency is not a simple task. As known, the poor performances of the integral action at frequencies different from zero leads to steady state error and to poor disturbance rejection, making the PI controller not suitable to track a sinusoidal current set point. Interesting solutions were presented in (Yuan et al., 2002), (Teodorescu et al., 2004). In these papers the authors develop the P+resonant (PR) controller for reference tracking in the stationary frame.
The use of control system in synchronous reference frame (d-q control), also for single-phase converters, was proposed for stand alone (Ryan & Lorenz, 1997), (Miranda et al., 2005) and for grid connected operations (Cacciato et al., 2008), (Bellini et al., 2008). In section 4 the d-q control is presented and the experimental results will show its nice performances.
Section 3 presents the topologies of PV systems, past and present technology, and the possible evolutions oriented towards the increase of the energy extracted by each PV module.

A very common topology for single-phase converters is the full-bridge with a line frequency transformer on the AC-side for galvanic isolation purposes. In this configuration the current injected into the grid is the transformer output current. Adopting this solution the DC current component at the transformer input is not directly controlled, and core saturation may appear producing current distortion. A simple solution to avoid core saturation issues is to control the current at transformer input instead of the injected grid current (Ciobotaru et al., 2005). However, this solution leads to lower power factor because of the presence of the transformer magnetizing current, especially at light load conditions. On the other hand, the direct control of the grid current requires a solution to saturation problems without introducing input transformer current measurement. In section 5 an original solution based only on injected current measurement is presented (Bellini et al. 2008). Experimental results show the effectiveness of the proposed method.
In new converter designs the tendency is to abandon line frequency transformers because of size, weight and price in favour of high frequency transformers. The presence of high frequency transformer requires several power stages and, as a consequence, increasing efficiency and reducing cost may be a hard task. In low power PV applications it is possible to remove the transformer at all in order to reduce losses, costs and size. The latter configurations are usually referred to as transformerless power converters. Without transformer coupling galvanic isolation between the grid and the DC source is lost and the big parasitic capacitance of the PV panel (Calais & Agelidis, 1998), (Calais et al, 2001) may introduce ground leakage currents.
Ground leakage currents increase conducted and radiated electromagnetic emissions, harmonics injected in the grid, losses and the converter has to be disconnected from the grid if the ground leakage currents exceed prefixed limits.
Section 6 reports the root causes of the ground leakage currents and some solutions. The best way to reduce them is the use of a suitable converter topology. Inside this section an original full bridge topology with unipolar PWM is presented that ensures a strong reduction of the leakage ground currents. Simulation results are reported that show the effectiveness of the proposed topology.

2. Maximum power exploitation of PV cells

The power generation from PV modules suffers from two main shortcomings: the efficiency of electric power generation is very low, especially under low radiation states (1), and the amount of electric power generated by solar arrays is always changing with weather conditions (2). Figure 1 shows the typical variations of the current voltage characteristic of a PV module respectively for different values of irradiance and working temperature. Figure 2 shows the equivalent circuit of a PV cell. A maximum power point tracking (MPPT) algorithm must operate in real-time in PV generation systems. The ideal MPPT algorithm sets the operating point of the PV panel, usually forcing the panel voltage at the Maximum Power Point (MPP). Figure 3 shows an example of the power-voltage characteristic of a photovoltaic field, composed by PV modules connected in series and in parallel for different values of irradiance and partial shading conditions.
Most of the MPPT algorithms are based on perturb and observe and on incremental conductance methods. Many improvements to these methods have been presented in order to improve the dynamic performances and to reduce undesired oscillations around the

MPP, (Femia et al., 2005), (Fangrui et al, 2008). In high power PV systems the ripple correlation control method can be used that is based on measuring and processing the current and/or voltage ripple created by the switching stage of the power converter (Esram et al., 2006).

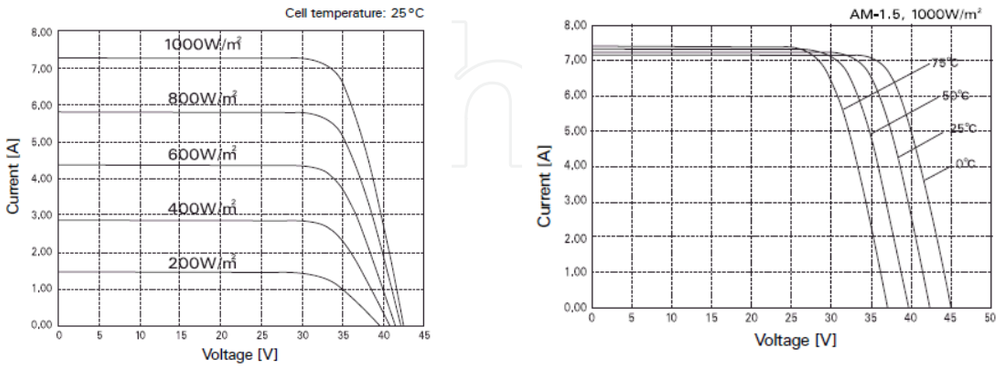

(a) (b)

Fig. 1. Electric characteristics of PV panels (Sanyo Photovoltaic HIP-230HDE1) for different values of irradiance and working temperature.

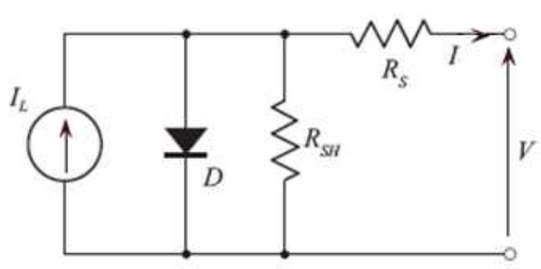

Fig. 2. Equivalent circuit of a PV cell.

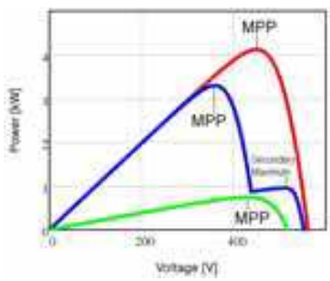

Fig. 3. Example of power-voltage characteristic of a photovoltaic field for different weather conditions.

In order to harvest the maximum energy the ripple at the terminals of the PV modules, must be minimized around the MPP. In single-phase converters since the instantaneous power does not equal the average power, there is an intrinsic fluctuation of the PV module output power at twice the frequency of the grid.

The reduction of the output ripple of the PV modules can be obtained only with a power decoupling device that is normally realized by means of large DC capacitors which decrease the lifetime and reliability of the whole system. The DC capacitors are either placed in parallel to the PV modules or to the dc link after a DC-DC converter used for voltage amplification.

In a three-phase system the instantaneous output power is constant and no DC large capacitors are needed leading to smaller cost and higher reliability with respect to single-phase inverters. The use of three-phase system also in low power applications could be an interesting solution for newer designs.

3. Topologies for grid connected photovoltaic systems

The basic elements of a PV system are the modules that are usually series-connected. A series of PV modules is usually called a PV string. If the voltage of the PV string is always higher than the peak voltage of the grid the PV converter does not require a step-up stage. In this case higher efficiency can be obtained because a single stage full-bridge converter can be used. Otherwise, a DC-DC converter or a transformer must be added for voltage amplification reducing efficiency. A PV system is the combination of PV fields and the related power converters.
The peak current that can be delivered by one string is determined by the PV module characteristics, figure 1. To achieve a higher power level several strings can be connected in parallel as shown in figure 4a. In this way, a single converter can be used reducing the cost and the losses of the static energy conversion. In this topology, usually referred to as Central Converter, the lack of individual MPPT for each string does not permit to harvest the maximum electric power from PV modules, especially when shading or different orientation of modules occurs. This major shortcoming results in avoiding this simple topology in newer photovoltaic system designs.

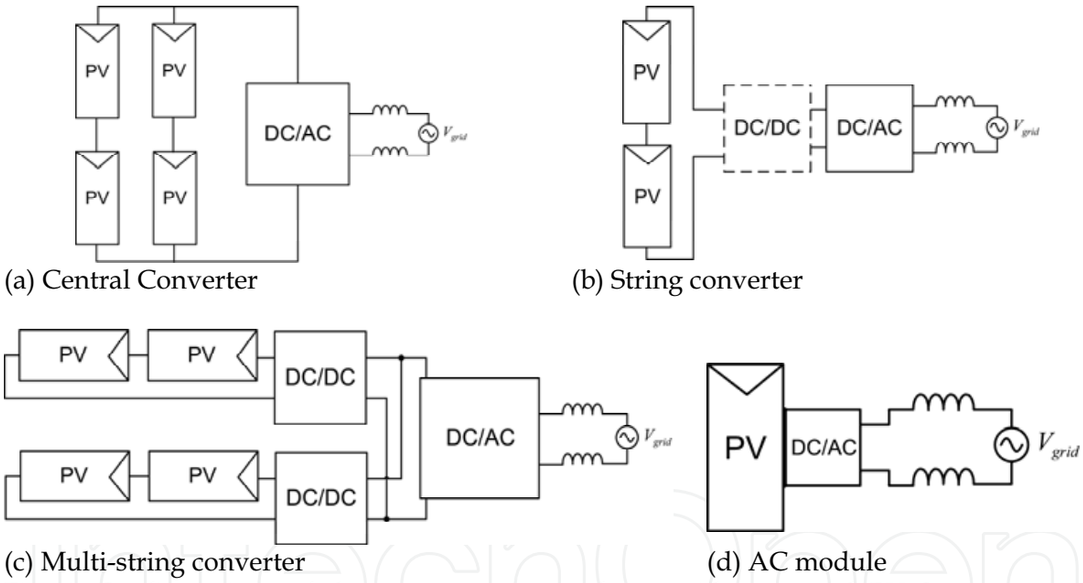

(a) Central Converter (b) String converter

(c) Multi-string converter (d) AC module

Fig. 4. Configurations of the power converter for a grid connected PV System, central converter (a), string converter (b), multi-string converter (c) and AC module (d).

Other options are possible as sketched in Figure 4. The string converter topology is shown in figure 4(b). This configuration does not employ the parallel connections of the strings. Each string has its own MPPT and is completely independent from each other. Therefore it is easy to build PV systems with different orientations, shading conditions and number of PV modules for each string.
A disadvantage of string-converters in comparison to central converters is the higher price per kW. String converters are often build only as single-phase converters due to the low power level. A very common classic topology is the full-bridge with a line frequency

transformer on the AC-side for galvanic isolation and for voltage step-up. This architecture is analyzed in section 5.
The multi-string converter (figure 4(c)) manages two or three strings, and provides independent MPPT by different DC-DC converters. In this case a two-stage configuration is mandatory. Thanks to these additional DC-DC stages, used also in some string converter, it is possible to obtain a very wide input voltage range which gives to the user big freedom in designing of the photovoltaic field.
In these topologies the modules of one string have to be well matched and should be installed in the same orientation to achieve a high energy harvest. The photovoltaic energy harvesting can be maximized by using an individual MPPT for each PV module. The low power level permits to integrate the converter into the housing of the PV module, that is called AC module (figure 4(d)). The AC module is connected directly to the grid and no DC wirings are needed between PV modules.
Despite their simple use and installation the low power level of AC modules leads to higher cost per watt. The major issue of this solution is the lifetime of the actual converters that is smaller than the lifetime of a PV module (20 years and more). When it will be comparable this solution will become interesting.

4. Current Controllers for Single-Phase Grid Connected Converters

4.1 d-q current controller

The DC-AC stage of a PV system must inject active grid current only, i.e. a pure sinusoidal current in phase with the grid voltage. To satisfy this condition the steady state error between the desired grid current and the actual one must be tightly zero at grid frequency. To this aim many control architectures have been presented in literature to overcome the drawbacks of the simple PI controller. As known, the poor performances of the integral action at frequency different from zero lead to steady state error and to poor disturbance rejection making the PI controller not suitable to track a sinusoidal set point in a stationary reference frame. The performances of PI controllers can be improved adding a feed-forward compensation to its output. The feed-forward value is computed in order to obtain at the output of the power converter the same voltage imposed by the grid in case of a zero contribution of the PI controller. The PI + feed-forward controller is used in some experimental results shown in section 6.
An interesting alternative is the P+resonant (PR) controller that introduces an infinite gain at a selected resonant frequency providing a theoretical zero steady-state error at that frequency. Actually the gain at resonant frequency is limited by stability problems.
A further option is the use of a control system in a reference frame synchronous with the grid frequency (d-q reference frame). The d-q control allows an infinite control loop gain at grid frequency and a superior disturbance rejection. Hence, it can increase efficiency cancelling reactive current delivered to the grid.
Mimicking the technique used in case of the single-phase transport delay PLL (Arruda et al, 2001), (Silva et al., 2004) to obtain the d-q current components in synchronous reference a current $i_\beta(t) = I\sin(\omega t + \varphi_i)$, orthogonal to the grid current $i_\alpha(t) = I\cos(\omega t + \varphi_i)$, is introduced. Appling the Park transformation I_d and I_q can be easily computed.

Let $v_\alpha(t) = V\cos(\omega t + \varphi_v)$ and $i_\alpha(t) = I\cos(\omega t + \varphi_i)$ be the grid voltage and the grid current, where ω is the grid pulsation, φ_v and φ_i are respectively the voltage and the current displacement, it holds:

$$\begin{bmatrix} I_d \\ I_q \end{bmatrix} = \begin{bmatrix} \cos\vartheta(t) & \sin\vartheta(t) \\ -\sin\vartheta(t) & \cos\vartheta(t) \end{bmatrix} \begin{bmatrix} i_\alpha \\ i_\beta \end{bmatrix} \tag{1}$$

where the angle $\vartheta(t) = \omega t + \varphi_v$ is obtained once the PLL is locked to the grid voltage angle. Matrix computations lead to the following results:

$$\begin{aligned} I_d &= I\cos(\varphi_v - \varphi_i) = I\cos\varphi \\ I_q &= -I\sin(\varphi_v - \varphi_i) = -I\sin\varphi \end{aligned} \tag{2}$$

Hence, I_d and $-I_q$ are respectively the amplitude of the active grid current, in phase with the grid voltage, and the amplitude of the reactive grid current, in quadrature with the grid voltage; $\cos\varphi$ is the power factor.

Being the system a single-phase one, only one manipulated variable can be managed. This variable, named in Figure 5 V_β, depends, generally speaking, on park transformation reference choice, and drives the single-phase DC/AC converter in order to obtain the desired grid current. V_β is a output of the Park inverse transformation, whose inputs are: 1) the V_d voltage, i.e. the output of the active current (I_d) control loop, 2) the V_q voltage, i.e. the output of reactive current ($-I_q$) control loop. The set-point of the reactive current control loop is set to zero because in ideal conditions only active current must be supplied.

A simpler choice would require only one current loop, fixing V_q=0. However, if the I_q control loop is opened, the presence of reactive voltage drops and system non ideal behavior will introduce a reactive current component and then a wrong current angle, as it will be shown in the following by simulation.

The right angle is achieved only if the reactive current loop is closed with a zero set-point. In fact, in ideal conditions, only the I_d current component must appear and the actual I_q current represents a measure of the system error.

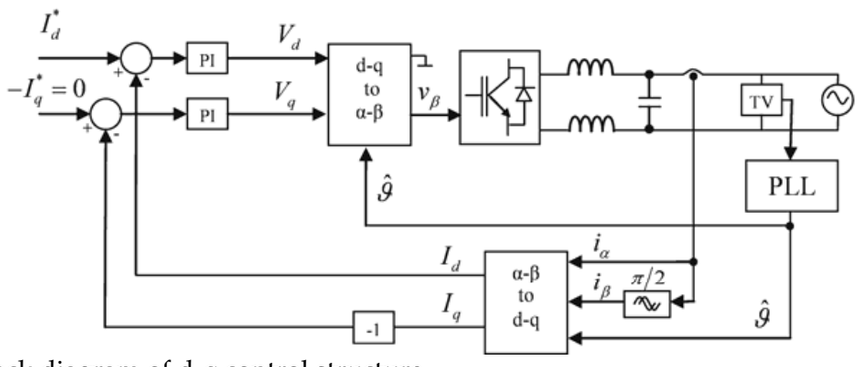

Fig. 5. Block diagram of d-q control structure.

4.2 Simulation Results

Numerical simulations were used to assess the performances of the proposed d-q control structure. The MATLAB simulink environment was used to model the whole system, where the power converter is modeled by PLECS toolbox. A fixed step time of 5 ms was used and all simulations refer to a step set-point of Id with an amplitude of 10A.

At first some simulations were made to verify the system performances in case of I_q current loop opened and V_q set to zero. In this case, the presence of the I_d control loop will fix the active grid current at the right value. However, because of reactive voltage drops and system non ideal behavior a reactive current component will appear and the grid current amplitude will increase beyond the desired level. Specifically, the synchronous reference frame control forces a zero steady state error in d-axis but this result is reached increasing the grid current amplitude instead of adjusting its angle.

Figure 6 shows the grid voltage and current under these conditions: the amplitude of the grid current is higher than requested because a remarkable amount of reactive current is injected into the grid. In these charts the grid current amplitude was amplified (x10) in order to identify easily the current displacement. The resulting power factor and then system performances are very poor.

Then simulations were made relying on the structure of figure 5. Thanks to the action of the I_q axis control loop the reactive current is forced to zero by integral action. Figure 7 shows clearly that only active current is now present. A unitary power factor is obtained and the amplitude of the grid current reaches its set-point (10A).

Figure 8 highlights the dynamic response of I_d and I_q: in a few periods d-q current control ensures zero steady state error as expected.

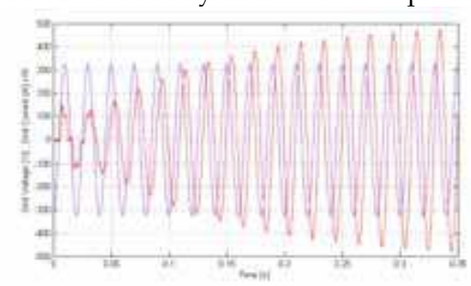

Fig. 6 Simulation results with simple control structure (V_q=0). Grid voltage (violet trace) and amplified (x10) grid current (red one).

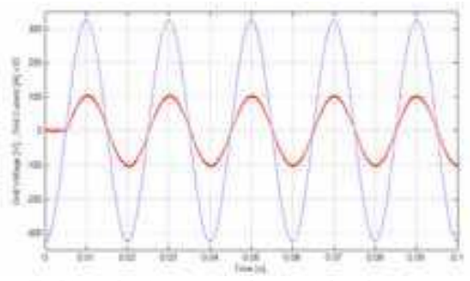

Fig. 7 Simulation results with d-q control. Grid voltage (violet trace) and amplified (x10) grid current (red one).

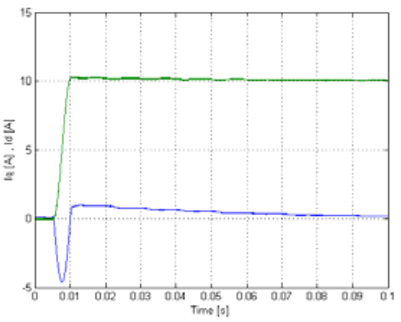

Fig. 8 Simulation results with d-q control. Dynamic response of I_d (green trace) and I_q (blue one).

4.3 Experimental Results

Several experiments were made in order to evaluate the performances of the d-q control. The designed prototype is based on a 56F8323 DSP that implements the control algorithm, the digital filtering, the grid synchronization, the reference frame transformation and the PWM modulation. Specifically a unipolar PWM modulation is adopted with a switching frequency of 10 kHz. The power stage is implemented on a 600 V, 25 A Intelligent Power Module (IPM). Using unipolar modulation a simple LC filter can be used with L = 2 mH, and C = 1.5 μF. The detailed design and optimization of the output filter is not investigated in this paper. A 400V low distortion DC voltage source was adopted.

Figure 9 and Figure 10 show the performances of the d-q control architecture. Figure 9 refers to a step set-point of I_d from 0 to 8A while the set point of I_q is fixed to zero. Under these conditions, the set-point is reached in about 10 ms, i.e. less than a period. The dynamic behavior of the currents is in a nice agreement with simulation results of Figure 8 and, as theoretically predicted, the d-q control keeps the current tightly at its set-point.

Figure 10 shows the steady state behaviour of the d-q control for a set-point of I_d = 7A. The injected grid current shows only a low distortion content in correspondence of voltage zero crossing.

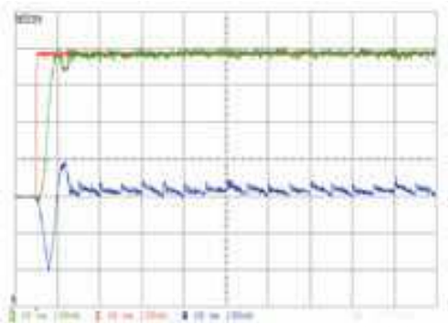

Fig. 9. Experimental Results. Step response: I_d (green solid line), I_q (blue solid line) and I_d^* set-point (red solid line).

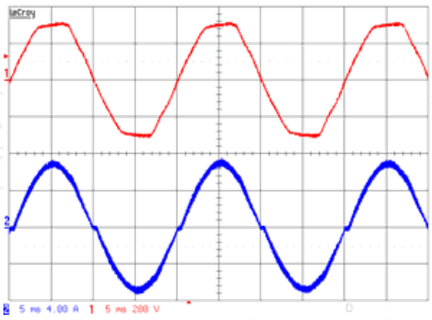

Fig. 10. Experimental Results. Stationary conditions: grid voltage (red solid line) and injected grid current (blue solid line).

5. Core saturation compensation strategies for PV power converters with line frequency transformers

5.1 Control of injected grid current in line frequency transformer PV converter

A very common topology for single-phase converters is the full-bridge voltage source inverter (VSI), driven by unipolar PWM, with a line frequency transformer on the AC-side for galvanic isolation (Figure 11). The line frequency transformer is a safe solution in order to match the electrical safety standards and to block out the DC current component. Moreover, it can be used to adjust the voltage level without requiring a DC/DC power converter. However, the transformer features increased size, weight, and price of the converter. The use of a toroidal transformer can partly reduce these drawbacks.

In order to achieve higher efficiency the inverter strategy control must inject only active grid current, i.e. a pure sinusoidal current in phase with the grid voltage. To this aim injected grid current must be controlled directly providing zero steady state error at grid frequency.

For a line frequency transformer PV converter, the control of the injected grid current stands for the control of the transformer output current. In this way, the DC current component at transformer input is not directly controlled and core saturation and thus current distortion may appear. A simple solution for avoiding core magnetic saturation, if current measurement is tuned properly, is to control the current at transformer input instead of the grid current. This solution leads to poorer performances at light loads conditions because of the transformer magnetizing current.

On the other hand, the direct control of the injected grid current without the measurement of current at transformer input is affected by saturation problems. In (Bellini et al. 2008) the authors presented a solution based only on injected grid current measurement.

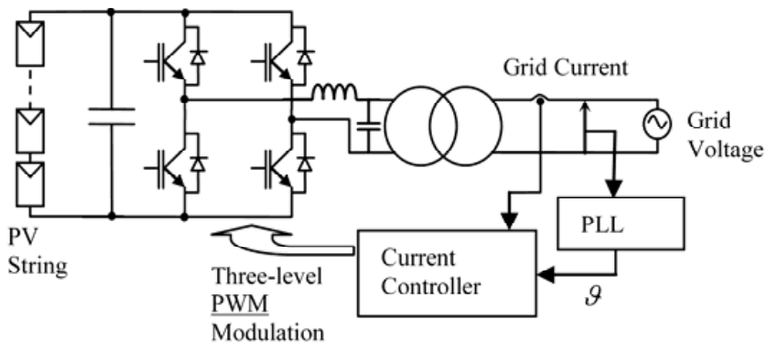

Fig. 11. Block diagram of a line frequency transformer PV converter.

If the control loop is closed at the transformer output a DC voltage and current bias may appear at the transformer input when a non ideal DC-AC converter feeds the transformer. In fact, the transformer blocks out the DC current component, hence the output current control is not able to manage the DC component at the transformer input. This bias can lead to magnetic core saturation and then to harmonic distortion of input and output currents. Figure 12 shows the effects of the DC voltage bias: the magnetic flux, that is, roughly, the integral of the voltage, will saturate asymmetrically. Depending on the sign of the bias, saturation will affect positive or negative semi-periods only. In correspondence of flux saturation the e.m.f. will decrease and the input current will increase accordingly, see Figure 12.

5.2 Saturation Compensation Strategy

In order to avoid core saturation and then current distortion a suitable algorithm was developed to compensate the DC bias effects. At first, the algorithm must identify the semi-period affected by saturation (i.e. the "sign" of saturation), then it must estimate its entity. Neglecting voltage drop across stray inductance the maximum and the minimum values of magnetic flux are synchronous with the zero crossings of the supply voltage waveform. Hence, it is expected that the effect of saturation will appear around zero crossings of supply voltage. Comparing the output current with its set-point value in correspondence of the zero crossings of supply voltage, two saturation indexes referred to as positive SI_P and negative SI_N values can be computed:

$$SI_P = \int_{\frac{T}{2}-\Delta T_{ZC}}^{\frac{T}{2}+\Delta T_{ZC}} \left| i^*_{grid} - i_{grid} \right| dt \tag{3}$$

$$SI_N = -\int_{T-\Delta T_{ZC}}^{T+\Delta T_{ZC}} \left| i^*_{grid} - i_{grid} \right| dt \tag{4}$$

where i_{grid} and i^*_{grid} are the actual grid current and the desired grid current waveform. From a theoretical point of view the time interval ΔT_{ZC} must be less then or, at least, equal to T/4. A time integration value of T/10 is sufficient to obtain a robust estimation of saturation core conditions.

The combination of SI_P and SI_N is a nice saturation estimator that can lead to an effective DC bias compensation as shown in the following. If a positive DC current component $I^+_{\mu 0}$ is superimposed to the current at transformer input, saturation affects the positive values of the flux, as reported in Figure 13. Hence the index SI_P will be positive while $SI_N = 0$. On the contrary, if a negative DC current component $I^-_{\mu 0}$ is present, saturation will affect the negative flux values. Hence $SI_P = 0$ and $SI_N > 0$. In case of absence of DC current component ($I_{\mu 0} = 0$), saturation is not present and $SI_P = SI_N = 0$. Computing and summing the two saturation indexes every period a rough estimation ($I_{\mu 0\_est}$) of DC current component can be made: $I_{\mu 0\_est} = SI_P + SI_N$.

Thanks to the estimation of $I_{\mu 0}$ the effect of the DC current component can be compensated with the simple feedback control detailed in Figure 14, where V^* is the output of the current regulator. The control loop forces a zero DC current component $I_{\mu 0}$ thus preventing magnetic saturation. This compensation strategy does not require DC current measurements, thus avoiding intrinsically transducer offset issues.

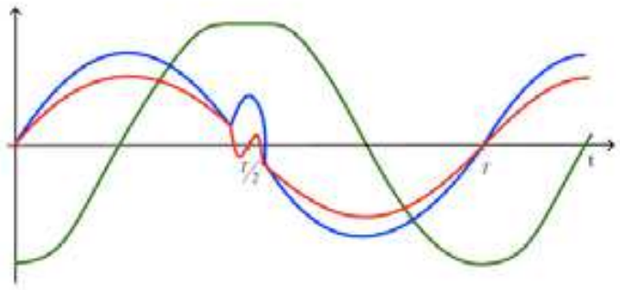

Fig. 12. Effect of a positive DC bias on the current at transformer input. Core flux (green solid line), transformer input (blue solid line) and output (red solid line) currents.

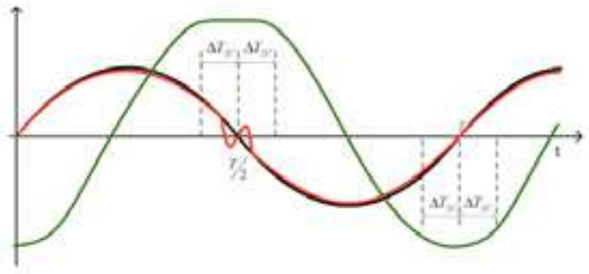

Fig. 13. Computation of saturation indexes. Core flux (green trace), current set point (black trace) and transformer output current (red one).

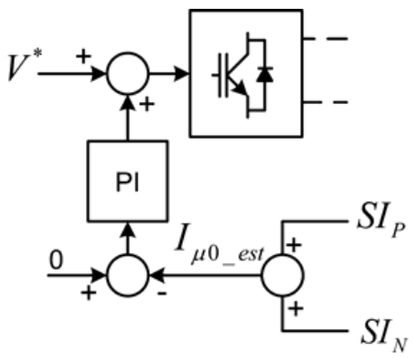

Fig. 14. Block diagram of the saturation compensation scheme.

5.3 Experimental Results

Several experiments were made in order to evaluate the performances of the saturation compensation strategy. Experiments were made with the prototype described in section 4.1. The saturation compensation strategy is applied to two different current controllers: PI+feed forward and d-q synchronous reference frame controllers. The amplitude of the desired grid current, i.e. the set-point of the current controller, is 8A in both cases.

Figure 15a shows the grid voltage, with an intrinsic distortion not correlated to the PV system, the grid current (transformer output current) and the transformer input current in case of PI regulator and feed-forward without saturation compensation. As it can be noted,

current distortion appears in correspondence of the voltage zero crossing at the end of a positive voltage semi-period, hence saturation is due to a positive DC bias at the transformer input. Figure 15b shows the effects of the saturation compensation strategy.

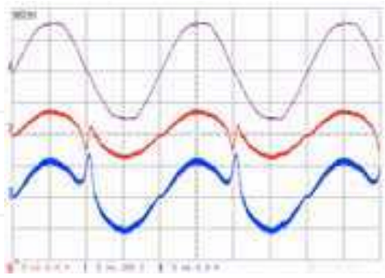

(a) PI regulator + feed forward control without saturation compensation

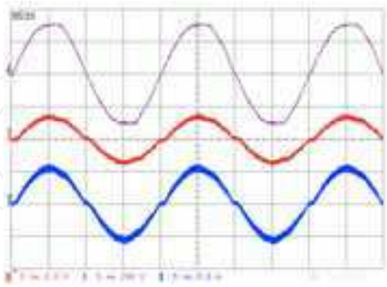

(b) PI regulator + feed forward control with saturation compensation

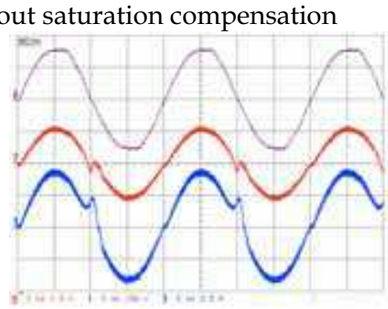

(c) d-q control without saturation compensation

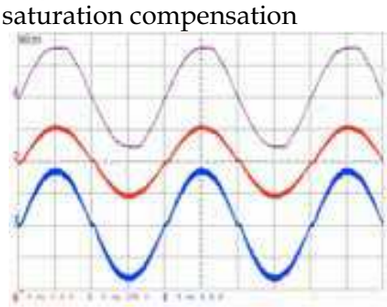

(d) d-q control with saturation compensation

Fig. 15. Experimental Results. Time waveforms of grid voltage (violet solid line), grid current (red solid line) and transformer input current (blue solid line).

The same experimental results are made using the d-q control without (Figure 15c) and with (Figure 15d) saturation compensation. As expected, in this case the steady-state error is zero and the better disturbance rejection of the d-q control damps harmonic distortion of the current. The proposed compensation strategy results very effective for both control schemes.

6. Transformerless grid-connected converters

In new converter designs the trend is to abandon line frequency transformers because of size, weight and price in favour of high frequency transformers. The presence of high frequency transformer requires several power stages and, as a consequence, increasing efficiency and reducing cost is a hard task.

In low power PV applications it is possible to remove transformer at all (transformerless configurations). The absence of the line frequency transformers does not ensure the elimination of DC grid current. The DC component is mainly caused by an offset in the grid current measurement that is usually realized through Hall effect sensors. As known, these sensors are strongly affected by DC offset drift. A current sensor based on fluxgate technology could be adopted to reduce the DC offset drift.

The absence of the line frequency transformer also causes two major drawbacks: safety issue in case of isolation faults, and wrong operation because of ground leakage currents.

The first issue occurs since the PV generator is not isolated from the grid, as a consequence isolation faults at the PV generator or at DC-wiring can get a safety hazard in case of indirect electric shock. Hence, transformerless inverters are equipped with Residual Current Devices (RCD), which monitor the ground leakage currents during operation. When a dangerous leakage current is recognized, the inverter is immediately disconnected from the AC-grid.
A typical configuration for a transformerless power converter, based on H-brige configuration, is reported in Figure 16.

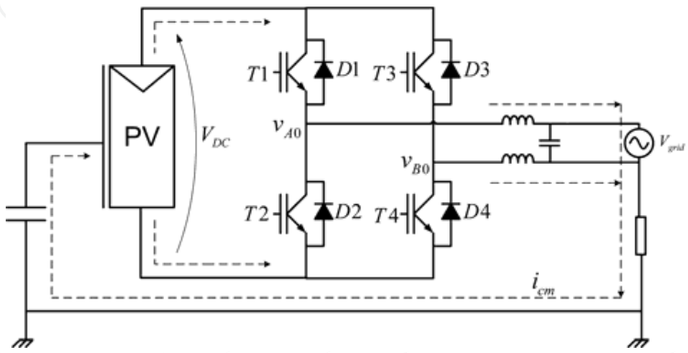

Fig. 16. Schematic representation of a transformerless power converter, based on H bridge, for PV systems. Leakage ground currents are shown as dashed lines.

The second issue is created by the large parasitic capacitance of the PV panel (10-100nF/kWp) that results in high ground leakage currents in case of variations of common mode voltage at the output of the power converter. Impulsive common mode voltages will result in large ground leakage currents because the power converter is coupled to a resonant circuit with a small damping coefficient. The resonant circuit is composed by the earth capacitance, the converter, the AC filter and the grid. A blocking filter is not easy to tune, since the earth capacitance changes with environmental conditions. The damping of the resonant circuit is small since it is mandatory to reduce dissipative terms and thus to achieve a high efficiency.
Therefore the best remedial strategy for ground leakage current is the reduction of the excitation, i.e. of variation of common mode voltage. To this aim it could be necessary to adopt topologies free from common-mode voltage variations (Lopez et al., 2007), (Gonzales et al., 2007). Converter topologies intrinsically safe from leakage currents are the Half-Bridge (HB) and the Neutral Point Clamped (NPC) ones (Gonzales et al., 2008), (Lopez et al., 2006). However, these configurations require twice the input voltage to obtain the same voltage level that is one of the major drawbacks for a PV system. On the other hand, a full-bridge converter driven by bipolar PWM (Gonzales et al 2007) exploits the full voltage rails but reduces common mode voltage with lower efficiency than HB of NPC configurations. From a power quality point of view all these solutions present current ripple at switching frequency.
For power converters with transformers the full bridge converter with unipolar PWM is widespread, since it represents a nice trade-off between efficiency, complexity and price. The biggest advantages of unipolar PWM are that the current ripple appears at twice the switching frequency and that the voltage across the AC output filter is unipolar, thus

reducing core losses. In summary, with unipolar PWM the maximum current ripple is four time smaller than the case of bipolar PWM. However, in terms of ground leakage currents the unipolar PWM generates common mode voltage at switching frequency with a peak to peak value equal to the DC voltage Bus. As a consequence, a big common-mode filter is required in photovoltaic transformerless applications relying on full bridge configurations with unipolar PWM.
Here an original architecture is proposed where a full bridge converter with a unipolar PWM is used with two additional blocks that ensure no common-mode voltage variations also in case of actual (asymmetrical) commutations.
The instantaneous common-mode voltage in the full-bridge converter of the Figure 16 can be computed from the two mid-points of both legs by:

$$v_{cm} = \frac{v_{A0} + v_{BO}}{2} \tag{5}$$

The most widespread single-phase topology is the full bridge one. This topology allows both bipolar and unipolar PWM. In the following sections the behavior of full bridge topologies with bipolar and unipolar PWM will be presented showing performances in terms of ground leakage currents and the original compensation circuitry.

6.1 Full bridge topologies with bipolar PWM for PV transformerless converters

Ideally, the full bridge converter with bipolar PWM does not generate a variation of common-mode output voltage. Hence, it is adopted in some commercial transformerless converters. With reference to the schematic of Figure 16 two configurations are sequentially operated in the switching cycle:

1) T1 and T4 ON (T2, T3 OFF): $v_{A0} = V_{DC}, v_{B0} = 0, v_{cm} = \frac{V_{DC}}{2}$

2) T2 and T3 ON (T1,T4 OFF): $v_{A0} = 0, v_{B0} = V_{DC}, v_{cm} = \frac{V_{DC}}{2}$

In case of ideally synchronous commutation of the switches the common-mode voltage is kept constant at half the DC bus level, and thus no ground leakage currents would appear. However, in actual converters, a small common-mode high-frequency filter is necessary to avoid ground leakage currents due to switching mismatch and asymmetries.
Recently modified version of the full bridge configuration with bipolar PWM were proposed in order to combine higher efficiency with reduced ground leakage currents in real operations.
Figure 17 presents a modified full-bridge topology with two additional blocks used alternatively: inserting only the DC decoupling block a former topology, known as H5, is obtained while, inserting the AC decoupling block a latter one, known as HERIC, is obtained (Kerekes et al., 2007), (Gonzalez et al., 2006). The use of DC or AC decoupling allows, during conduction of freewheeling diodes, the disconnection of the grid from photovoltaic panel.

If no conduction of freewheeling diodes occurs the power switch of DC Decoupling in H5 topology is on while the power switches of the AC decoupling in HERIC topology are off. The H bridge is driven according to 1) and 2) and common mode voltage will be equal to $V_{DC}/2$. On the other side during conduction of freewheeling diodes H5 topology modifies the PWM involving only the high side of the bridge. DC decoupling is OFF hence, in case of symmetrical commutations $v_{A0} = v_{B0} = V_{DC}/2$. In this way common mode voltage does not vary avoiding ground leakage currents increase.
The HERIC topology obtains the same result turning on one of the two added power switches of the AC decoupling block in function of the sign of the injected grid current and driving off the transistors of the H bridge. So doing the freewheeling will involve only the AC Decoupling.
In both topologies the output voltage is zero during freewheeling obtaining a three level output voltage as in case of unipolar modulation. However the output current ripple is still at switching frequency.
Again asymmetrical PWM commutations can determine little leakage ground currents.

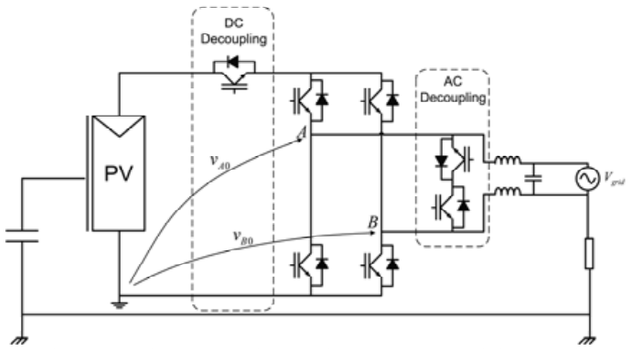

Fig. 17. Full Bridge topology with DC and AC decoupling additional blocks.

6.2 Full bridge topology with unipolar PWM for PV transformerless converters

The full bridge topology with unipolar PWM ensures a reduction of the current ripple, specifically the maximum current ripple is four times smaller then the bipolar PWM maximum current ripple.
Referring to Figure 16 the common-mode voltage resulting during a switching cycle in case of unipolar PWM is computed in the following. Reference is made to positive output voltage and current (first quadrant operations); output voltage is indicated as $v_{AB} = v_{A0} - v_{B0}$.
Four configurations are sequentially operated in the switching cycle:

1) T1, T4 On (T2, T3 OFF): $v_{AB} = V_{DC}$, $v_{cm} = \frac{V_{DC}}{2}$.

2) T2, T4, D2 ON: $v_{AB} = 0$. Low side current freewheeling through D2, T4, $v_{cm} = 0$.

3) T1,T4 On (T2, T3 OFF): $v_{AB} = V_{DC}$, $v_{cm} = \frac{V_{DC}}{2}$.

4) T1, T3, D3 ON: $v_{AB} = 0$. High side current freewheeling through T1, D3, $v_{cm} = V_{DC}$.

The common mode voltage v_{cm} varies from 0 to V_{DC} and thus a large ground leakage current will flow.

Figure 18 shows the original configuration that is proposed to reduce ground leakage currents. Two additional blocks are added: the former one, named DC decoupling, fixes the common mode voltage to $V_{DC}/2$, while the latter, named No-Ideality compensation, helps to keep a constant common mode voltage in case of non ideal (asymmetrical) commutations.

The DC decoupling disconnects the H-bridge from DC source during freewheeling. In particular during high side freewheeling T5 is switched off while during low side freewheeling T6 is switched off. In case of ideal commutations this block is sufficient to guarantee no variations of the common mode voltage v_{cm}. In actual converter, to fix the v_{cm} at $V_{DC}/2$ during asymmetrical commutations, two additional low power switches should be added. In order to avoid the complexity introduced by two controlled switches an attempt was made replacing them with two diodes. The idea relies on the following explanation. Once the decoupling switch T5 opens, the voltage of the high side of the H bridge, is floating. Then this voltage, due to parasitic capacitances, would decrease, however the inserted diode will clamp it to $V_{DC}/2$. Simulation results confirm this behavior.

Since the two diodes impose a maximum voltage equal to $V_{DC}/2$ across T5 and T6, latest generation Mosfets can be chosen as controlled switches, in order to reduce the power losses.

In figure 18 x and y represent the PWM signals used for driving the legs of the full bridge. A simple combination of PWM signals can be used for driving the switches of DC decoupling block.

With reference to the schematic of Figure 18 four configuration are sequentially operated in the switching cycle:

1) T1, T4, T5,T6 ON (T2 and T3 OFF): $v_{AB} = V_{DC}$, $v_{cm} = \frac{V_{DC}}{2}$.

2) T2, T4, T5, D2 ON (T1, T3, T6 OFF): $v_{AB} = 0$. Low side current freewheeling through T4, D4, $v_{cm} = v_{A0} = v_{B0} = \frac{V_{DC}}{2}$.

3) T1, T4, T5, T6 ON (T2 and T3 OFF): $v_{AB} = V_{DC}$, $v_{cm} = \frac{V_{DC}}{2}$.

4) T1, T3, T6, D3 ON (T2, T4, T5 OFF): $v_{AB} = 0$. High side current freewheeling through T1,D3, $v_{cm} = v_{A0} = v_{B0} = \frac{V_{DC}}{2}$.

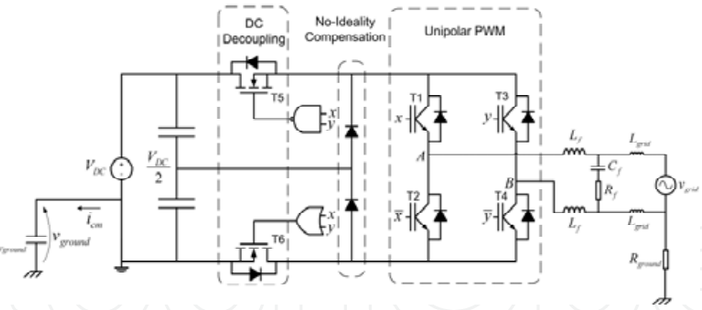

Fig. 18. Schematic of the original configuration for full bridge topology with unipolar PWM for transformerless converters.

In an actual converter the PWM modulation strategy of the DC decoupling block has to be modified because of the presence of dead times. A simple adaptation of the driving circuit can be made that ensures correct operations in actual conditions.

6.3 Simulation Results

The proposed topology (Figure 18) was validated thanks to the PLECS toolbox, which allows fast simulation of power electronic circuits under MATLAB/Simulink. The simulation parameters are: $V_{DC} = 450V$, $V_{grid} = 230V_{rms}$, $R_{ground} = 2\Omega$, $C_{PVground} = 14nF$, $L_f = 2mH$, $C_f = 2.2\mu F$, $R_f = 0.5\Omega$, $L_{grid} = 40\mu H$, the switching frequency is $f_{sw} = 10kHz$. A simple current controller is used to inject a sinusoidal current of $13A_{rms}$ into the grid with unitary power factor equivalent to 3kW of injected active power.

Extensive simulations were performed with the attempt to assess the performances of the proposed converter topology with special reference to common mode voltage and ground leakage currents. Results confirm that the proposed topology allows to keep the common voltage constant at $V_{DC}/2$. In this way, the resulting ground leakage currents are negligible.

Figures 19, 20, 21 show respectively the common mode voltage v_{cm} , the ground voltage v_{ground} and the ground leakage currents i_{cm} without DC decoupling and No-Ideality compensation additional blocks. These simulations were made to quantify the common mode voltage and the ground leakage currents arising in a transformerless full bridge topology with unipolar PWM. Figures 22, 23 show the simulation results obtained when the two additional blocks are added. Figure 22 shows that the common mode voltage v_{cm} is fixed to $V_{DC}/2$. Therefore the ground voltage v_{ground} does not contain high frequency components and only the fundamental grid frequency is present (Figure 22). The resulting leakage ground currents will be very small, as shown in Figure 23.

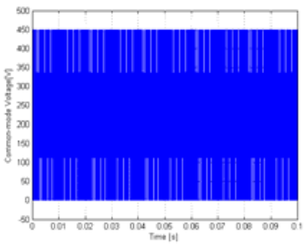

Fig. 19. Simulation results. Common mode voltage in a transformerless unipolar PWM full bridge converter.

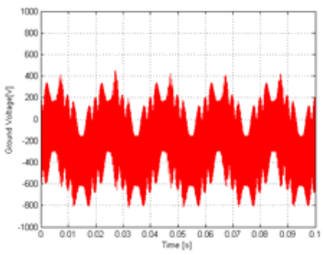

Fig. 20. Simulation results. Ground voltage in a transformerless unipolar PWM full bridge converter.

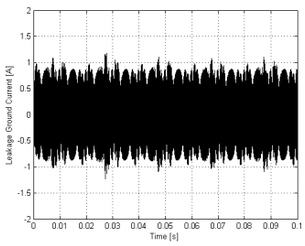

Fig. 21. Simulation results. Ground leakage current in a transformerless unipolar PWM full bridge converter.

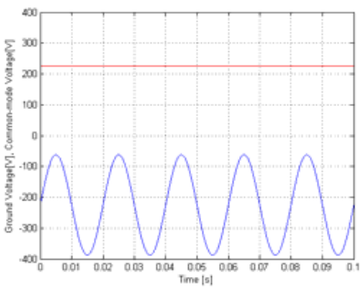

Fig. 22. Simulation results. Common mode voltage (red trace) and ground voltage (blue trace) with the proposed topology.

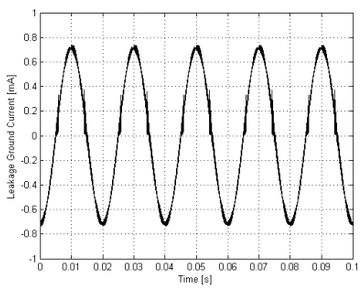

Fig. 23. Simulation results. Ground leakage currents [mA] with the proposed topology.

7. Conclusion

This chapter deals with single-phase grid connected converters used in photovoltaic plants. Some proposed improvements to the widespread full bridge topology are investigated in order to improve energy conversion.

PV power converters, based on full bridge topology, are distinguished by the presence or not of a line frequency transformer.

In both cases the control of the injected grid current is one of the most important issue. The d-q current controller was deeply analyzed and some experimental results are reported to show its superior power quality in comparison with traditional controllers.

In order to increase the performances, notably at light loads conditions, the full bridge topology was modified moving the feedback from the transformer input to the transformer output. In this way, the DC component at the transformer input is not directly controlled, thus an original core compensation strategy is proposed to avoid saturation. Experimental results are reported showing the effectiveness of the proposed compensation.

In low power applications the trend is to remove the transformer (transformerless configurations) in order to reduce losses, costs and size.

In transformerless configurations the major issues are the accurate control of DC component of injected grid current, the safety issues in case of isolation faults, and the reduction of

ground leakage currents. Here the most common configurations are reviewed and an original solution is presented that achieves a nice trade-off between efficiency, power quality and reduction of ground leakage currents.

8. References

Chung, S.K. (2000). Phase-Locked Loop for Grid-Connected Three-Phase power conversion systems, *IEE Proc. – Electr. Power Appl*., Vol. 147, No. 3, pp. 213-219.

Arruda, L. N.; Cardoso Filho, B. J.; Silva, S. M. & Diniz, S.A.C. (2001). Wide bandwidth single and three-phase PLL structures for grid-tied PV systems, *in Proc. of EPE'01*, pp. 1660-1663.

Silva, S.M.; Filho, B.C.; Campana, R.P. & Boaventura, W.C (2004). Performance evaluation of PLL algorithms for single- phase grid-connected systems, *in Proc. of IAS'04*, vol. 4, pp. 2259 - 2263. C. J. Kaufman, Rocky Mountain Research Lab.

Yuan, X.; Merk, W.; Stemmler, H. & Allmeling, J. (2002). Stationary-frame generalized integrators for current control of active power filters with zero steady-state error for current harmonics of concern under unbalanced and distorted operating conditions. *IEEE Transactions on Industry Applications*, vol. 38, no. 2, pp. 523–532, Mar./Apr. 2002.

Teodorescu, R.; Blaabjerg, F.; Borup, U. & Liserre M. (2004). A new control structure for grid-connected LCL PV inverters with zero steady-state error and selective harmonic compensation, *in Proc. of Applied Power Electronics Conference and Exposition, 2004*. APEC '04. Nineteenth Annual IEEE, vol. 1, pp. 580–586.

Ryan, M. J. & Lorenz R. D. (1997). A synchronous-frame controller for a single-phase sine waveinverter. *in Proc. Of Applied Power Electronics Conference and Exposition*. APEC '97 Conference Proceedings 1997., Twelfth Annual, vol. 2, Atlanta, GA, USA, Feb. 1997, pp. 813–819.

Miranda, U. A.; Rolim, L. G. B. & Aredes M. (2005). A DQ synchronous reference frame current control for single-phase converters, *in Proc. Of Power Electronics Specialists Conference*. PESC '05. IEEE 36th, 2005, pp. 1377–1381.

Cacciato, M.; Consoli, A.; Aiello, N.; Attanasio, R.; Gennaro, F. & Macina G. (2008). A digitally controlled double stage soft-switching converter for grid-connected photovoltaic applications, in Proc. *Of Applied Power Electronics Conference and Exposition*. APEC 2008. Twenty-Third Annual IEEE, Feb. 2008, pp. 141–147.

Bellini, A.; Franceschini, G.; Lorenzani, E. & Tassoni, C. (2006). Synchronous reference frame grid current control for single-phase photovoltaic converters, *in Proc. of IAS 2008*, pp 1 – 7, Edmonton (Canada), October 5-9 2008

Ciobotaru, M.; Teodorescu, R. & Blaabjerg, F. (2005). Control of single-stage single-phase PV inverter, *in Proc. of Power Electronics and Applications*, 2005 European Conference on, Sept. 2005.

Calais, M. & Agelidis, V. G. (1998). Multilevel converters for single-phase grid connected photovoltaic systems—An overview, *in Proc. IEEE Int. Symp. Ind. Electron.*, vol. 1, pp. 224–229.

Calais, M.; Myrzik, J. M. A. & Agelidis, V. G. (2001). Inverters for single phase grid connected photovoltaic systems—Overview and prospects, *in Proc. 17th Eur. Photovoltaic Solar Energy Conf.*, Munich, Germany, Oct. 22–26, pp. 437–440.

Kuo, Y. C.; Liang, T. J. & Chen, J. F. (2001). Novel maximum-power-pointtracking controller for photovoltaic energy conversion system, *IEEE Trans. Ind. Electron.*, vol. 48, no. 3, pp. 594–601, Jun. 2001.

Femia, N.; Petrone, G.; Spagnuolo, G. & Vitelli, M. (2005). Optimization of perturb and observe maximum power point tracking method, *Power Electronics, IEEE Transactions on* , vol.20, no.4, pp. 963-973, July 2005

Fangrui Liu; Shanxu Duan; Fei Liu; Bangyin Liu & Yong Kang,(2008). A Variable Step Size INC MPPT Method for PV Systems, *IEEE Transactions on Industrial Electronics,* vol. 55, no. 7, pp. 2622-2628, July 2008

Esram, T.; Kimball, J.W.; Krein, P.T.; Chapman, P.L. & Midya, P. (2006). Dynamic Maximum Power Point Tracking of Photovoltaic Arrays Using Ripple Correlation Control, *IEEE Transactions on Power Electronics*, vol. 21, no.5, pp. 1282-1291, Sept. 2006

Lopez, Oscar; Teodorescu, Remus; Freijedo, Francisco & Doval-Gandoy, Jesus (2007). Leakage current evaluation of a singlephase transformerless PV inverter connected to the grid, *Applied Power Electronics Conference, APEC 2007* - Twenty Second Annual IEEE ,pp. 907 – 912, Feb. 25 2007-March 1 2007

Gonzalez, R.; Lopez, J.; Sanchis, P. & Marroyo, L. (2007). Transformerless Inverter for Single-Phase Photovoltaic Systems, *IEEE Transactions on Power Electronics* Volume 22, Issue 2, March 2007, pp. 693 – 697.

Gonzalez, R.; Gubia, E.; Lopez, J. & Marroyo, L. (2008). Transformerless Single-Phase Multilevel-Based Photovoltaic Inverter, *IEEE Transactions on Industrial Electronics* Volume 55, Issue 7, July 2008, pp. 2694 – 2702.

Lopez, Oscar; Teodorescu, Remus & Doval-Gandoy, Jesus.(2006). Multilevel transformerless topologies for single-phase grid-connected converters, *IEEE IECON 2006* - 32nd Annual Conference on Nov. 2006, pp. 5191 – 5196.

Kerekes, T.; Teodorescu & R.; Borup, U. (2007). Transformerless Photovoltaic Inverters Connected to the Grid, *Applied Power Electronics Conference, APEC 2007* - Twenty Second Annual IEEE Feb. 25 2007-March 1 2007, pp.1733 – 1737.

Gonzalez, R.; Lopez, J.; Sanchis, P.; Gubia, E.; Ursua, A. & Marroyo, L. (2006). High-Efficiency Transformerless Single-phase Photovoltaic Inverter, *Power Electronics and Motion Control Conference, 2006. EPE-PEMC 2006*, 12th International Aug. 2006, pp. 1895 – 1900.

Renewable Energy
Edited by T J Hammons

ISBN 978-953-7619-52-7
Hard cover, 580 pages
Publisher InTech
Published online 01, December, 2009
Published in print edition December, 2009

Renewable Energy is energy generated from natural resources-such as sunlight, wind, rain, tides and geothermal heat-which are naturally replenished. In 2008, about 18% of global final energy consumption came from renewables, with 13% coming from traditional biomass, such as wood burning. Hydroelectricity was the next largest renewable source, providing 3% (15% of global electricity generation), followed by solar hot water/heating, which contributed with 1.3%. Modern technologies, such as geothermal energy, wind power, solar power, and ocean energy together provided some 0.8% of final energy consumption. The book provides a forum for dissemination and exchange of up-to-date scientific information on theoretical, generic and applied areas of knowledge. The topics deal with new devices and circuits for energy systems, photovoltaic and solar thermal, wind energy systems, tidal and wave energy, fuel cell systems, bio energy and geo-energy, sustainable energy resources and systems, energy storage systems, energy market management and economics, off-grid isolated energy systems, energy in transportation systems, energy resources for portable electronics, intelligent energy power transmission, distribution and inter-connectors, energy efficient utilization, environmental issues, energy harvesting, nanotechnology in energy, policy issues on renewable energy, building design, power electronics in energy conversion, new materials for energy resources, and RF and magnetic field energy devices.

How to reference
In order to correctly reference this scholarly work, feel free to copy and paste the following:

Emilio Lorenzani, Giovanni Franceschini, Alberto Bellini and Carla Tassoni (2009). Single-Phase Grid Connected Converters for Photovoltaic Plants, Renewable Energy, T J Hammons (Ed.), ISBN: 978-953-7619-52-7, InTech, Available from: http://www.intechopen.com/books/renewable-energy/single-phase-grid-connected-converters-for-photovoltaic-plants

INTECH
open science | open minds

InTech Europe
University Campus STeP Ri
Slavka Krautzeka 83/A
51000 Rijeka, Croatia
Phone: +385 (51) 770 447
Fax: +385 (51) 686 166
www.intechopen.com

InTech China
Unit 405, Office Block, Hotel Equatorial Shanghai
No.65, Yan An Road (West), Shanghai, 200040, China
中国上海市延安西路65号上海国际贵都大饭店办公楼405单元
Phone: +86-21-62489820
Fax: +86-21-62489821

IntechOpen